DETECTION OF BUILDING DAMAGE AREAS DUE TO THE 2006 CENTRAL JAVA, INDONESIA EARTHQUAKE USING HIGH-RESOLUTION SATELLITE IMAGES

H. Miura[1] and S. Midorikawa[2]

[1] *Assistant Professor, Dept. of Built Environment, Tokyo Institute of Technology, Yokohama, Japan*
[2] *Professor, Dept. of Built Environment, Tokyo Institute of Technology, Yokohama, Japan*
Email: hmiura@enveng.titech.ac.jp, smidorik@enveng.titech.ac.jp

ABSTRACT :
Rapidly quantifying extent and severity of building damage is a high priority in an aftermath of a large earthquake. In this study, a semi-automated damage detection technique is applied to high-resolution satellite optical images observed before and after the 2006 Central Java, Indonesia earthquake (Mw6.3). The satellite FORMOSAT-2 images whose spatial resolution is 2m are used. In the damage detection, the difference of digital numbers between pre- and post-earthquake images is mainly utilized. The distribution of the pixels detected by the proposed method is compared with actual damage distribution evaluated from the result of visual detection of satellite images and the damage statistics. The result shows that the distribution of the detected pixels approximately corresponds to the severely damaged areas.

KEYWORDS: Damage detection, High-resolution satellite image, Spectral reflectance, The 2006 Central Java earthquake

1. INTRODUCTION

In order for emergency response and early recovery assessment after a large-scale disaster, it is important to rapidly comprehend extent and severity of building damage. Remote sensing technology would be useful to widely identify building damage areas without field survey. In the Central Java, Indonesia earthquake (Mw6.3) on May 27, 2006, severe building damage was observed in and around Yogyakarta city. About 5,800 people were killed and 38,000 people were injured due to the earthquake. About 140,000 houses were completely collapsed, and 190,000 houses were severely damaged.

Damage distribution maps were estimated using remote sensing data observed after the earthquake [e.g., UNOSAT, 2006 and RESPOND, 2006]. The maps were delineated based on visual detection of high-resolution satellite images such as QuickBird images. The visual detection, however, requires a great demand for labor and the results depend on skills of the operators. Automated or semi-automated damage detection technique is necessary to quickly identify damaged areas for more rapid post-earthquake assessment. In this study, a building damage detection method is applied to satellite optical images observed before and after the 2006 Central Java earthquake, and the validity of the method is discussed.

2. CHARATERISTICS OF SATELLITE IMAGES

2.1 Pre- and Post-Earthquake FORMOSAT-2 Images

Images of the satellite FORMOSAT-2 launched by Taiwan in May 2004 are used in this study. The satellite provides a panchromatic (black/white) image whose spatial resolution is 2m and a multi-spectral (color) image whose resolution is 8m. The multi-spectral image consists of four bands (Band1: Blue (B), Band2: Green (G), Band3: Red (R), and Band4: Near infrared (NIR)). The off-nadir view angle of the satellite is constant, while the

view angles of other high-resolution commercial satellite such as QuickBird and IKONOS are often changed from observation to observation in order to capture a target area in a short time interval. The constant view angle would make it easier to precisely overlay a pair of images acquired in different date. Besides, the image width of FORMOSAT-2 is about 25km, while the width of the other high-resolution satellite images is only 10-15km. These are advantages of FORMOSAT-2 images in widely detecting changes between pre- and post-event.

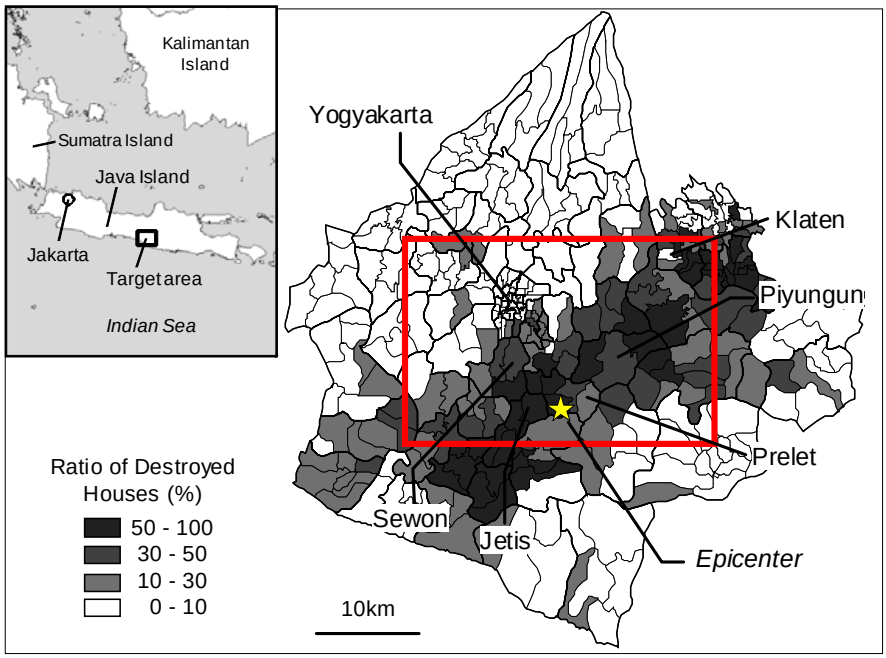

Figure 1 Coverage of FORMOSAT-2 image (Red square) and damage distribution in the 2006 Central Java earthquake

Figure 1 shows the map of the epicentral area of the 2006 Central Java earthquake with the distribution of the damage ratio compiled by the regional officials [International Federation of Red Cross, 2006]. Solid square indicates the area of the FORMOSAT-2 image used in this study. Figures 2 show the true color images observed before and after the earthquake. The color images are pan-sharpened to 2m spatial resolution using the panchromatic images and the multi-spectral images. The characteristics of the images such as the observation dates, the satellite angles and the sun angles are shown in Table 1. The pre-event image was observed nine days before the earthquake and the post-event image is acquired fifteen days after the earthquake. The time interval of the images is about 1 month.

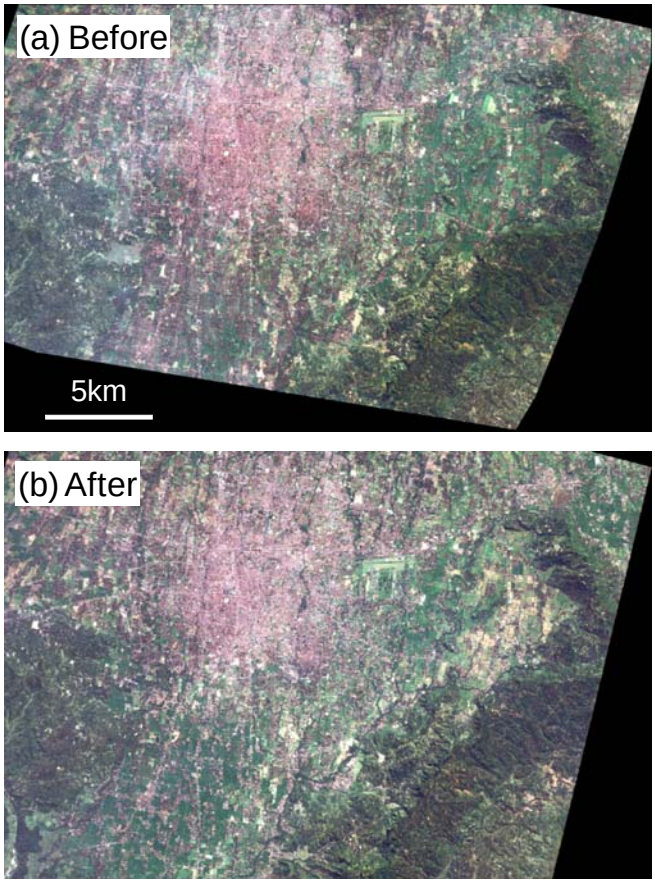

Figures 2 Pre- and post-earthquake FORMOSAT-2 images used in this study

2.2 Spectral and Spatial Characteristics of Damaged Area

The close-ups of the pre- and post-earthquake images are shown in Figs. 3. The cross-sections of digital numbers (DN) along the dotted line in the images are also illustrated in the lower part of Figs. 3. Black lines and red lines indicate the digital numbers of pre- and post-event images, respectively. Figure 3(a) represents the close-up of a severely damaged settlement. As shown by the cross-sections, the digital numbers in the damaged area after the earthquake is higher than those before the earthquake. In the severely damaged area, numbers of wall bricks and debris of buildings are exposed on the ground

Table 1 Characteristics of FORMOSAT-2 images

Event	Date	Time	Satellite		Sun		Spatial Resolution (m)
			Azimuth (deg.)	Elevation (deg.)	Azimuth (deg.)	Elevation (deg.)	
Before	May 18, 2006	AM 09:09	N103.2E	28.8	N52.3E	44.9	2.0
After	Jun 11, 2006	AM 09:09	N102.8E	28.5	N48.7E	42.2	2.0

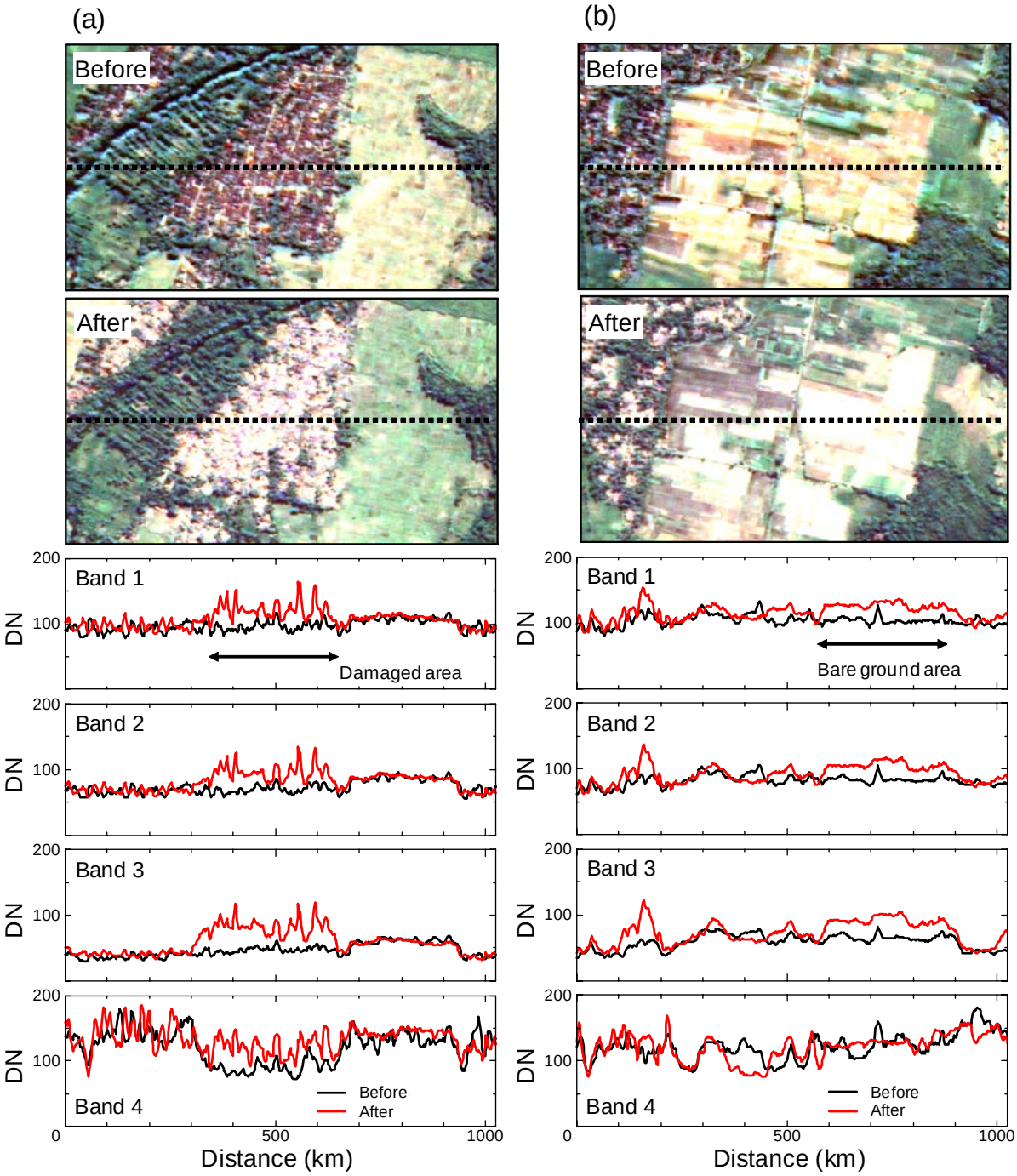

Figures 3 Close-ups of images and cross-section of digital numbers
(a) Severely damaged area, (b) Bare ground area

surface due to the collapse of buildings. The difference of the digital numbers between the images would be caused by the difference of spectral reflectance of building materials.

Figure 4 show the spectral reflectance of typical building materials observed during the field survey in Central Java area [Miura *et al.*, 2007]. The horizontal axis indicates wavelength in nanometer and the vertical axis indicates reflectance in percentage. The reflectance is computed as the ratio of irradiance of the target material divided by irradiance of referenced white plate. The spectral coverage (B, G, R and NIR) of the FORMOSAT-2 image is also shown as horizontal bars in Fig. 4. Higher spectral reflectance of objects produces higher digital number in the satellite image. The spectral reflectance of a brick is higher in red and near infrared band than those of a roof tile and asphalt. As mentioned before, wall bricks of damaged buildings are exposed on the ground surface in the severely damaged area. These would be the reasons why the digital numbers in the damaged area become higher than those before the earthquake. The result suggests a possibility to identify damaged areas from difference of the digital numbers between the images.

Figure 3(b) shows the close-up of a bare ground area where rice paddies are cropped. The comparison of pre- and post-earthquake images shows that the digital numbers in the bare ground area after the earthquake are higher than that before the earthquake. This may be because that the soil moistures are temporally changed in different observation dates. When the damaged areas are detected by differencing of digital numbers between the images, it is necessary to discriminate damaged areas from bare ground areas. The comparison of the cross-sections in Figs. 3(a) and (b) show that the shape of the digital numbers in the damaged area is more jagged than that in the bare ground area. Spatial variations such as texture information of the image would be helpful to discriminate damaged areas from bare ground areas. Since the difference of digital numbers in the band 3 (Red) is larger than the other bands, the band 3 images are mainly used in the following steps.

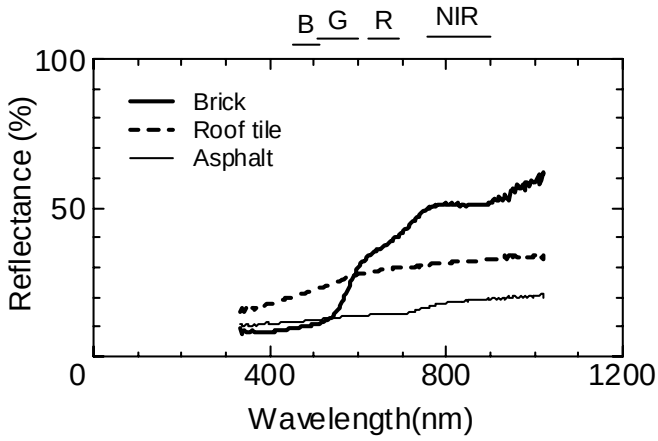

Figure 4 Spectral reflectance of typical building materials [Miura et al., 2007]

3. DETECTION OF BUILDING DAMAGE AREAS

3.1 Methodology

Flowchart of proposed damage detection method is shown in Fig. 5. Firstly, the pre-earthquake image is geometrically corrected to superpose the post-earthquake image. The pixels of the image are broadly classified into three categories; vegetated area, bare ground area, and built-up area. The vegetated areas such as paddy fields, grasses and forests are extracted using NDVI (Normalized difference vegetation index) computed from the post-earthquake images. NDVI is computed by the equation (1) shown below.

$$NDVI = (DN_{NIR} - DN_{Red}) / (DN_{NIR} + DN_{Red}) \quad (1)$$

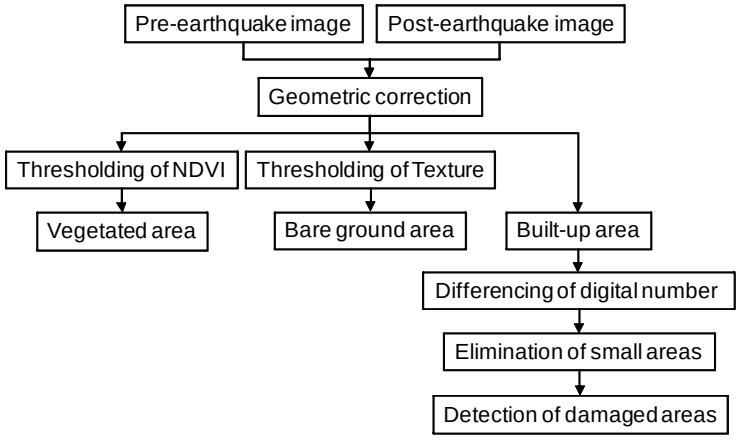

Figure 5 Flowchart for detection of damaged areas

Here, DN_{NIR} and DN_{Red} represent digital number of a pixel in the near infrared band and the red band image, respectively. NDVI is related to the amount of biomass within a pixel and yields a number from −1 to +1. A higher NDVI indicates a higher density of green leaves. Figures 6(a) and (b) show the close-up of damaged area in the post-earthquake image and the distribution of NDVI computed from the image, respectively. By comparing the distribution of the vegetation with that of NDVI, the threshold value to distinguish vegetated area from other area is determined. In this study, the pixels whose NDVI is higher than 0.4 are classified into vegetated area. Black pixels in Fig. 6(b) indicate the determined threshold value.

Bare ground areas are extracted using variance of digital numbers that is one of the texture information. The variance of digital numbers is computed for 7 by 7 pixel windowed area. The distribution of the variance is shown in Fig. 6(c). The figure shows that the variance in the settlements is larger than the bare ground areas and the vegetated areas. The threshold value to distinguish bare ground area from built-up area is determined by comparing the distribution of bare ground areas with that of the variance. The pixels whose variances are lower than 10 in the post-earthquake image are classified into bare ground areas. The other pixels are classified into built-up areas.

The difference of the digital numbers between the pre- and post-earthquake images is computed for the pixels classified into built-up areas. The threshold value to distinguish damaged area from undamaged area is determined from the distribution of the difference of digital numbers between obviously damaged areas and

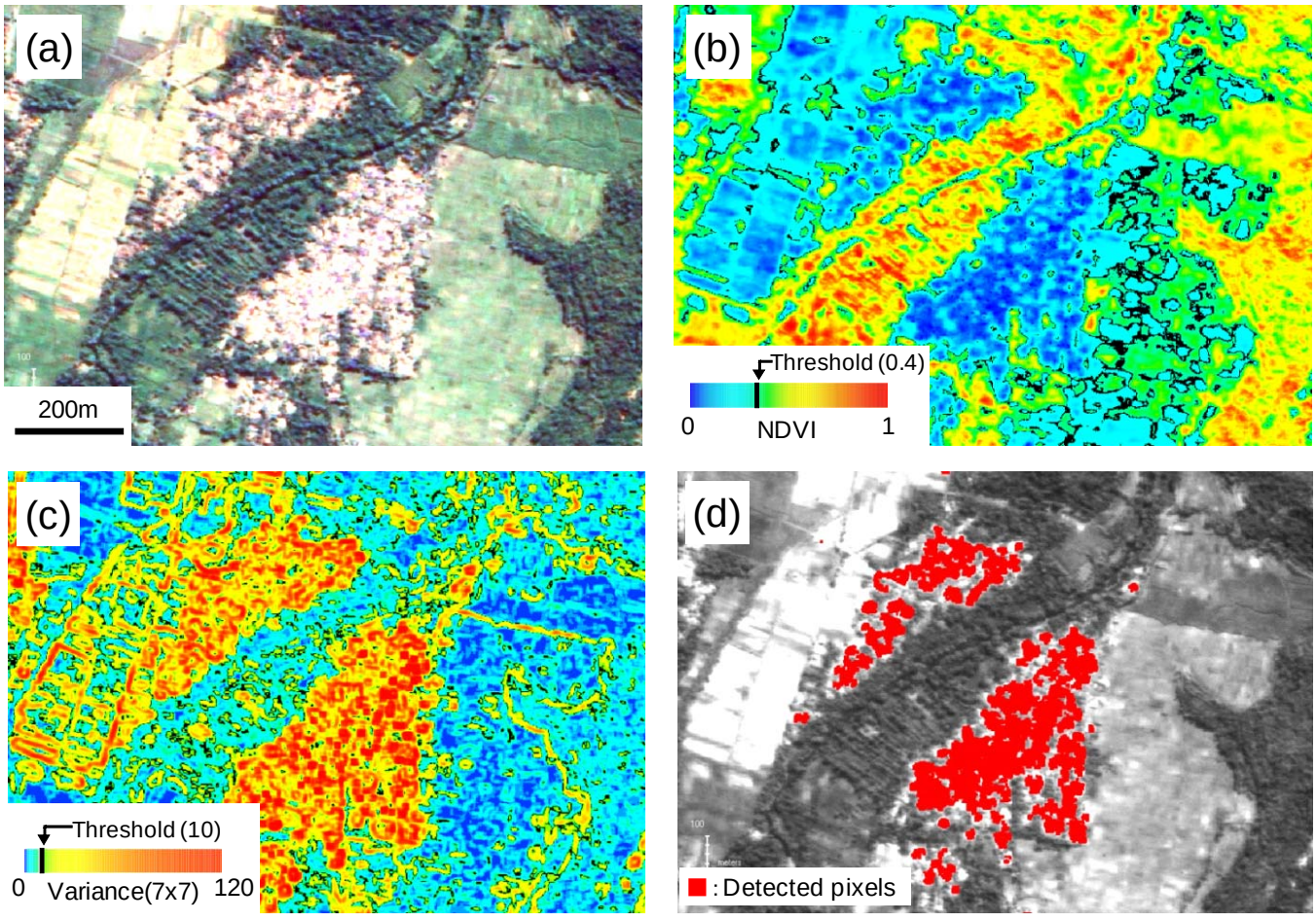

Figures 6 (a) Close-up of severely damaged area, (b) Distribution of NDVI,
(c) Distribution of variance, (d) Distribution of detected pixels

undamaged areas. In this study, the pixels whose difference of digital numbers is higher than 20 are extracted as damaged areas. Finally, in order to reduce small-scale mid-detections, small areas of the detected pixels are eliminated. The pixels whose area is less than 200 m^2 (50 pixels) are classified into small areas to be eliminated. Figure 6(d) shows the distribution of the finally detected pixels. The comparison of the result (Fig. 6(d)) and the original image (Fig. 6(a)) shows that the severely damaged areas are well detected by the proposed method.

3.2 Distribution of Actual Building Damage

In order to discuss validity of the proposed method, the distribution of the actual building damage is evaluated. The UNOSAT estimated the damage map by using high-resolution satellite images such as QuickBird images [UNOSAT, 2006]. The damage areas were visually detected from the images. The damage distribution is shown by color areas in Fig. 7(a). In the map, the damage is classified into three categories; extensive damage (red), moderate damage (orange), and limited damage (yellow).

Statistics of the building damage are also used to evaluate the damage distribution. The statistics were compiled by the regional officials of Yogyakarta and Central Java and includes total population, number of households, and number of damaged houses in each village [International Federation of Red Cross, 2006]. The building damage was classified into three categories; destroyed, heavy damage, and slight damage. The damage ratio is computed from the number of destroyed houses divided by the number of households in each village. Figure 7(a) also shows the distribution of the damage ratio by gray scale, indicating that the darker villages are the higher damaged areas.

The actual damage distribution is evaluated by combining the damage maps by the UNOSAT and by the damage statistics. As shown in Fig. 7(a), most of the extensive and moderate damage by the UNOSAT map is concentrated in Prelet and Jetis. Besides, the damage ratios in these areas are mostly higher than 50%. These results indicate that these areas are the severest damaged region. The moderate and limited damage by the UNOSAT is distributed in Sewon and Piyungun. The damage ratios in these areas are higher than 30% and 50%, respectively. The damage is expanded to Klaten because the damage ratios are higher than 50%. On the UNOSAT map, however, the damage was not delineated in Klaten because the satellite images used in the visual detection do not cover this area. From the combination of these damage distributions, the severely damaged areas are broadly grouped into four regions as shown by dotted circles in Fig. 7(a). The largest circle covers Jetis and Prelet. The other three circles cover Sewon, Piyungun and Klaten, respectively.

3.3 Evaluation of Damage Detection

The distribution of the damaged areas estimated by the proposed method is shown in Fig. 7(b). Red pixels indicate the detected areas. The dotted circles that indicate severely damaged areas are also illustrated in Fig. 7(b). The comparison of the detected areas with the actual damage distribution shows that most of the detected pixels are concentrated in the dotted circles. Especially, many pixels are detected in the largest circle area such as Jetis and Prelet, indicating the similarity with actual damage distribution. The damage is detected also in Klaten by the proposed method. The distribution of the detected pixels approximately corresponds to the severely damaged areas.

Many pixels, however, are detected also in Depok located in the northern part of the target area. Because the damage ratio in Depok is smaller than 10%, most of these pixels would be mis-detections. The comparison of the detection and the original images shows that most of the mis-detected pixels are undamaged buildings whose roof colors are bright. The digital numbers of these buildings are high in both pre- and post-earthquake images. Even in undamaged buildings, digital numbers between the images are slightly fluctuated. One of the reasons for the mis-detections might be that the fluctuation of the digital numbers in buildings with bright roof is larger than that in buildings with dark roofs.

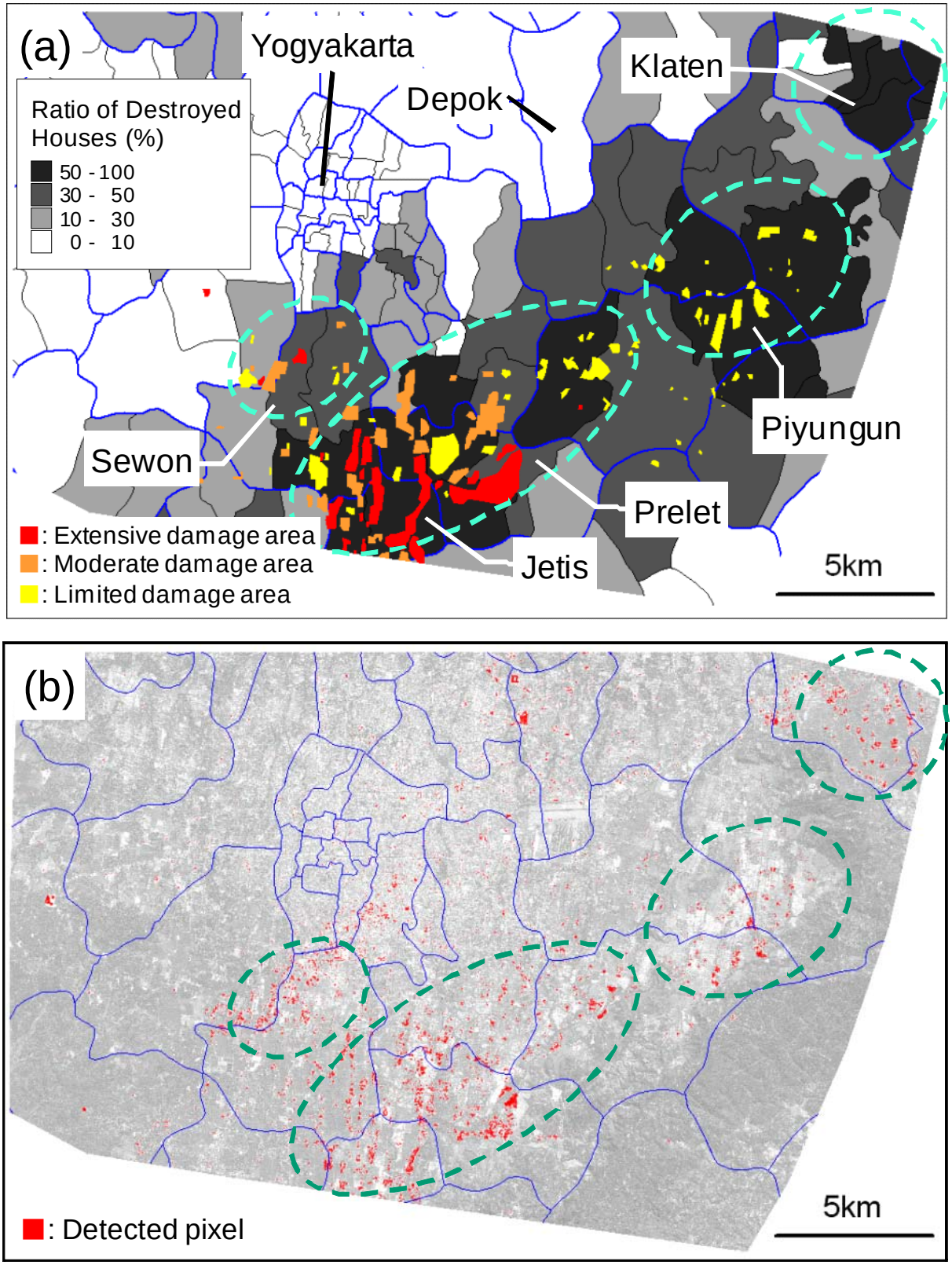

Figures 7 (a) Damage distribution by the UNOSAT [UNOSAT, 2006] (color scale) with distribution of damage ratio computed from damage statistics [IFRC, 2006] (gray scale),
(b) Distribution of pixels detected by proposed method.

4. CONCLUSIONS

A methodology to semi-automatically detect building damage areas is introduced and applied to the FORMOSAT-2 images observed before and after the 2006 Central Java, Indonesia earthquake. Using NDVI and variance of the digital numbers, the pixels of the image are classified broadly into three categories; vegetated area, bare ground area and built-up area. The damaged areas are detected from the difference of the digital numbers in the built-up areas between the pre- and post-earthquake images. The distribution of the pixels detected by the proposed method is compared with the actual damage distributions by the visual detection of high-resolution satellite images and by the damage statistics. The result shows that the distribution of the detected pixels approximately corresponds to the severely damaged areas.

ACKNOWLEDGMENT

This study is supported by the 21st Century COE Program "Evolution of Urban Earthquake Engineering" sponsored by Ministry of Education, Culture, Sports, Science and Technology (MEXT), Japan.

REFERENCES

International Federation of Red Cross (IFRC). (2006). Damage, Distribution and Preliminary Needs Assessment, http://www.reliefweb.int/library/documents/2006/IFRC/ifrc-idn-20jun.xls.

Miura, H., Yamazaki, F. and Matsuoka, M. (2007). Identification of Damaged Areas due to the 2006 Central Java, Indonesia Earthquake Using Satellite Optical Images, *Proceedings of Urban Remote Sensing Joint Event*, Paper No.DIS4.

RESPOND. (2006). Damage Assessment of the Earthquake on May 27, 2006, http://www.respond-int.org.

UNOSAT. (2006). Preliminary Damage Assessment: Java Earthquake, http://unosat.web.cern.ch/unosat/asp/.